

Article

Comparative Study of Zn Loading on Advanced Functional Zeolite NaY from Bagasse Ash and Rice Husk Ash for Sustainable CO₂ Adsorption with ANOVA and Factorial Design

Patchaya Tobameekul ¹, Supawon Sangsuradet ¹ and Patcharin Worathanakul ^{1,2,*}

¹ Department of Chemical Engineering, Faculty of Engineering, King Mongkut's University of Technology North Bangkok, 1518 Pracharat 1 Road, Wongsawang, Bangsue, Bangkok 10800, Thailand; s5801031910011@email.kmutnb.ac.th (P.T.); s6101031910016@email.kmutnb.ac.th (S.S.)

² Center of Eco-Materials and Cleaner Technology (CECT), Science and Technology Research Institute, King Mongkut's University of Technology North Bangkok, 1518 Pracharat 1 Road, Wongsawang, Bangsue, Bangkok 10800, Thailand

* Correspondence: patcharin.w@eng.kmutnb.ac.th; Tel.: +66-2-555-2000 (ext. 8242)

Abstract: The objectives of the research were to develop synthesis and estimation of each factor on carbon dioxide adsorption of advanced functional zeolite NaY material derived from bagasse ash and rice husk ash with different crystallization temperatures and weight percentages of zinc by the ion exchange method. The adsorbents were tested in a packed bed reactor at different temperatures and flow rates of carbon dioxide. The Minitab program was used to estimate the effects of each factor on carbon dioxide adsorption properties. The results showed that extracted silicon dioxide from bagasse ash and rice husk ash could be successfully used as raw material for zeolite NaY synthesis with a crystallization temperature of 298.15 K. The zeolite NaY crystalline structure was well-preserved after ion exchange. The highest capacity of carbon dioxide adsorption was at 10.33 mmol/g with zeolite 5B298-373-1. The results of the Minitab program showed that the carbon dioxide adsorption decreased with increasing crystallization temperature and carbon dioxide flow rate parameters. However, the increased weight percentage of zinc loading on zeolite NaY resulted in better carbon dioxide adsorption. The factors of the types of adsorbents and adsorption temperature showed interaction with each other.

Keywords: bagasse ash; rice husk ash; zeolite NaY; zinc loading; carbon dioxide; statistical analysis



Citation: Tobameekul, P.; Sangsuradet, S.; Worathanakul, P. Comparative Study of Zn Loading on Advanced Functional Zeolite NaY from Bagasse Ash and Rice Husk Ash for Sustainable CO₂ Adsorption with ANOVA and Factorial Design.

Atmosphere **2022**, *13*, 314. <https://doi.org/10.3390/atmos13020314>

Academic Editors: Kumar Vikrant and Dimitrios Giannakoudakis

Received: 31 December 2021

Accepted: 11 February 2022

Published: 13 February 2022

Publisher's Note: MDPI stays neutral with regard to jurisdictional claims in published maps and institutional affiliations.



Copyright: © 2022 by the authors. Licensee MDPI, Basel, Switzerland. This article is an open access article distributed under the terms and conditions of the Creative Commons Attribution (CC BY) license (<https://creativecommons.org/licenses/by/4.0/>).

1. Introduction

Biomass resources are waste from the food industry, crop by-products, and agricultural wastes such as rapeseed, water caltrop shell, lotus stalk, hazelnut shell, sawdust, bagasse ash, and rice husk ash [1–5]. Thailand is the world's second-largest exporter of sugar and rice [6,7]. Thailand produces approximately 14.58 million tons of sugar per year and 20.72 million tons of rice per year [8]. The steps involved in sugar mill processing are as follows: juice extraction, purification, crystallization, centrifugation, and drying [9,10]. The residue bagasse 26% of sugarcane is a by-product after juice extraction. Bagasse is a biomass fuel that is used in boilers to create steam for turbine generators. The burning process is transformed into thermal energy for power generation in sugar industries. After burning, bagasse ash is a residue that contains about 0.62% by weight of sugarcane [11–13]. In addition, after paddy rice is milled and rice husk is an essential by-product of the rice milling process [14,15]. Rice husks are classified as biomass fuel. Rice husk is also used as a fuel in boilers for biomass power plants. Rice husk ash is a classified solid waste that accounts for about 20% of the weight of rice husk. Rice husk ash is lightweight, which holds a direct impact on the environment and human respiratory problems [7,16–18]. Consequently, decreasing the amount of bagasse ash and rice husk ash is still a concern that needs to be addressed properly.

The large amounts of bagasse ash and rice husk ash are rich in silica. Therefore, various studies have been conducted to add value of these materials [19,20]. However, one of the solutions described above is silica extraction from bagasse ash and rice husk ash for producing a low-cost silica source [21,22]. Previous research has used bagasse ash and rice husk ash for catalyst synthesis, such as mesoporous silica and zeolite [15,17,23]. There is the potential to reduce waste disposal and pollution issues [24,25].

Nevertheless, air pollution is also emitted from industries and power plants that burn fossil fuels such as coal, oil and natural gas [26,27]. This emitted air pollution is known as a greenhouse gas, which includes carbon dioxide (CO₂), methane (CH₄), nitrous oxide (N₂O), chlorofluorocarbons (CFCs), hydrofluorocarbons (HFCs), perfluorocarbons (PFCs) and sulfur hexafluoride (SF₆). Among all of them, CO₂ is the major contributor to global warming and continually rising global temperatures [28–30]. By the year 2100, CO₂ concentrations in the atmosphere will have steadily climbed from pre-industrial levels of 280 ppm to 570 ppm [31–38]. To help reduce global warming, CO₂ adsorption in the post-combustion stage is essential. Adsorbents directly impact the performance of the adsorption method [39]. Various types of adsorbents are used for CO₂ adsorption, such as mesoporous silica materials, activated carbon, metal-organic framework, MCM-41 and zeolites [33,40–47].

Zeolite is one of the excellent adsorbents for CO₂ adsorption. Research for zeolite synthesis is becoming increasingly popular. Because zeolite is a crystalline porous material, it possesses a high surface area and molecular pore structure, and is thermally and mechanically stable [36,48–50]. The zeolite NaY from the faujasite family is the focus of this research because it exhibits a solid acidity, a three-dimensional pore structure and a highly molecular sieve. The channel of zeolite NaY is formed by the 12-member oxygen rings with a pore size diameter of 7.4 Å. Moreover, it can be synthesized at a low Si/Al ratio (0.75–3.8) compared to other zeolites. As a result, zeolite NaY can be modified to improve the efficiency of adsorption using the ion exchange method, allowing it to be able to absorb high amounts of CO₂ [51].

In general, a biomass power plant released flue gases containing dust, water, SO_x, NO_x, CO and CO₂. After the pretreatment process, the flue gases are mainly composed of CO₂. However, a temperature above 573.15 K is emitted from the power plant, depending on the design and process operation [52,53]. Nevertheless, CO₂ adsorption at high temperatures required high energy consumption, resulting in an expensive method. Consequently, it is necessary to develop zeolites for CO₂ adsorption at high temperatures in order to improve the efficiency of zeolites and to reduce the cost of CO₂ adsorption. The development of zeolites is influenced by the synthesis conditions and their cations contained [54].

Modification of the surface, such as chemical vapor deposition and impregnation methods, as well as ion exchange by the solid-state and aqueous solution, can improve the structural properties of zeolites and reduce the poor properties [51,55]. According to the research of Worathanakul and Rakpasert [50,55], Cu (II) and Ni (II) were successfully incorporated into zeolite Y using the ion exchange and impregnation method. The zeolite Y structure is unaffected by Cu (II) and Ni (II) loading in both techniques. Metal oxides such as Fe, Ni, Cu and Zn are widely utilized in combination with various zeolite types. It could help to improve acidity as well as hydrophobic-hydrophilic properties [46]. In addition, Esquivel and his colleagues [56] showed the CO₂ adsorption of Zn (II) loading on zeolite beta. Smykowski and his colleagues [57] studied the adsorption of CO₂ on DOH zeolite with varying the metal type from Cu, Zn, Ni, Pd. They proposed that the Zn cation interacts more strongly with CO₂ molecules than other cations, resulting in greater CO₂ adsorption. This is due to Zn that modifies the surface charge characteristics of zeolites by creating Lewis acidic sites and redox features. In the literature on adsorbent modification, there is no mention of Zn-exchanged zeolite NaY for CO₂ adsorption. Furthermore, Zn is an especially suitable option because Zn possesses a higher combustion temperature than 723.15 K. Therefore, the zeolite support is combined with Zn to achieve better CO₂ adsorption efficiency at high temperatures [25].

Therefore, factors for synthesis and conditions for CO₂ adsorption are important for this study. Minitab is a computer program that is designed to perform the processing of statistics with regression, multivariate analysis, factor analysis, principal components, qualitative data, time series and some nonparametric analysis [58–64]. The Minitab software was used to analyze the experimental data in order to measure the effects of various factors. The design determined effects on a response as well as how the effect of one factor varied with the level of the other factors [65,66]. Moreover, this method allows for identifying the extent of the influence of factors, while reducing the number of tests required for elucidation. Statistical analysis was performed to acquire the data that resulted in the factors examined [63].

The objectives of this research were to develop an advanced functionally zeolite NaY material synthesized from bagasse ash and rice husk ash for CO₂ adsorption to get better air quality management. NaY zeolites from bagasse ash and rice husk ash were used with a Si/Al ratio of 0.75 with different crystallization temperatures and weight percentages (wt.%) of Zn using the ion exchange method. Zeolite NaY after ion exchange was used as an adsorbent in a packed bed reactor at different temperatures and flow rates for CO₂ adsorption. Finally, the Minitab program was used to estimate the effects of modified functionally adsorbents, adsorption temperature and CO₂ flow rate. Furthermore, the goal of this research was to develop and apply knowledge in industrial for CO₂ adsorbent materials as well as to reduce air pollution.

2. Materials and Methods

The synthesis and analysis of zeolite NaY from rice husk ash and bagasse ash for CO₂ adsorption included five important steps: silica preparation, zeolite NaY synthesis, ion exchange, CO₂ adsorption, and statistical analysis.

2.1. Materials

The material used for silica preparation and zeolite NaY synthesis was followed by rice husk ash with 70.19 wt.% SiO₂ (U-Thong Biomass Co., Ltd., Suphanburi, Thailand) and bagasse ash with 70.81 wt.% SiO₂ (Khonburi Sugar Public Co, Ltd., Nakhon Ratchasima, Thailand). Other materials used were sodium hydroxide (99 wt.% NaOH, Merck, Darmstadt, Germany), hydrochloric acid (37 wt.% HCl, Merck, Darmstadt, Germany), sodium aluminate (NaAlO₂, 50–56 wt.% Al₂O₃, 40–45 wt.% Na₂O and 0.05 wt.% Fe₂O₃, Sigma Aldrich, Singapore), distilled water and deionized water (DI). As a metal loading, zinc nitrate (99.5 wt.% Zn (NO₃)₂•6H₂O, Merck, Darmstadt, Germany) was used. Carbon dioxide (CO₂ 99.80%: HP Grade, Linde, Bangkok, Thailand) was used in a continuous flow system with a packed bed for CO₂ adsorption.

2.2. Silica Extraction Derived from Bagasse Ash and Rice Husk Ash

The bagasse ash was initially dried at 378.15 K for 12 h. Ten grams of bagasse ash was then mixed with NaOH solution (2 molar) and stirred at 343.15 K for 1 h to extract silica. After that, the obtained solutions were filtered. The filtrates were titrated with HCl solution to adjust pH to 7 and then the solution started to form a gel. The solution was left at 298.15 K until the silica solidified. The solidified silica-rich was cleaned with DI water and filtered to separate the silica-rich solid residue. The silica solid was then dried overnight to obtain silica in the form of sodium silicate (Na₂SiO₃) for zeolite NaY synthesis. The above methods were repeated with rice husk ash as a silica source.

2.3. Zeolite NaY Synthesis

The zeolite NaY was synthesized according to a previously reported procedure with different crystallization temperatures and times [55]. The zeolite NaY was prepared with a Si/Al ratio of 0.75 and consisted of four steps, including seed gel, feedstock gel, overall gel and crystallization, along with Rakpasert (2012) [67]. She has reported that the zeolite NaY formed at temperatures higher than 343.15 K and 1 h exhibited better crystallinity,

while crystallization at temperatures lower than 343.15 K and 1 h revealed a low degree of crystallinity, resulting in poorly crystallized samples. It still needs to reduce the time and temperature of the synthesis as short as possible while maintaining at high quality. Therefore, heat crystallization at 298.15, 323.15 and 343.15 K was chosen to obtain a synthesis with lower energy consumption and higher efficiency. The seed gel step was initially prepared by mixing with NaOH and distilled water. The solution was then divided into two bottles and the NaAlO₂ and Na₂SiO₃ from bagasse ash were added while stirring and heating for 2 h. The second step is feedstock gel, in which the NaAlO₂ and Na₂SiO₃ solutions were produced in the same way under different volumes. The third step is the overall gel that the seed gel solution was slowly mixed into the feedstock gel solution under stirring until homogenous. The solution was left overnight at 298.15 K to form a gel. The final step is crystallization, in which the gel was heated with three different crystallization temperatures for 1 h. After that, the samples were cleaned with distilled water until pH 9 and filtered. The residue was then dried overnight to obtain zeolite NaY. The above methods were repeated with Na₂SiO₃ from rice husk ash for zeolite NaY synthesis. The zeolite NaY synthesized from different raw materials and crystallization temperatures was denoted as zeolite SC. S is the type of silica source (B = bagasse ash and R = rice husk ash); C is the crystallization temperature (298, 323 and 343).

2.4. Zn Loading to Zeolite NaY

Previous studies examined aspects of adsorbent modification; there is no mention of Zn exchanged zeolite NaY for CO₂ adsorption. However, Worathanakul and Saisuwanisri [68] studied and compared the CO₂ adsorption of Cu and Fe loading on zeolite Y, varying the wt.%. 5 wt.% Cu and 1 wt.% Fe loading on zeolite Y. The results showed a high CO₂ conversion of 67.06 and 61.14%, respectively. Therefore, Zn loading on zeolite NaY at 1, 3 and 5 wt.% was selected to develop a novel approach with desirable adsorption capacity properties. Ion exchange of the zeolite was then performed in different wt.% with 1, 3 and 5 wt.% of Zn loadings. One gram of the obtained zeolite NaY was added to a solution of 1 wt.% of zinc nitrate and stirred overnight at 298.15 K. The solutions were cleaned with DI water and filtered. After that, the residue was then dried overnight at 393.15 K. The sample was calcined at 873.15 K for 5 h in the air to obtain the modified zeolite NaY powder. The above methods were repeated with 3 and 5 wt.% of Zn for modified zeolite NaY powder. The adsorbent samples were denoted as zeolite XSC. Where X represents the wt.% of Zn in the total weight of the sample.

2.5. CO₂ Adsorption Test

In general, a biomass power plant releases flue gases containing dust, water, SO_x, NO_x, N₂, CO and CO₂. In the present study, dust, water, acidic gases and volatile organic compounds were assumed to be removed during the pretreatment process (i.e., electrostatic precipitation, dehumidification, desulfurization and de-NO_x). Because various components could be found in effluent gases, multi-component adsorption is experimentally too complicated. After the pretreatment process, the flue gases are mainly composed of CO₂. Since the adsorption of pure CO₂ on applied adsorbents is essential for well-designed adsorption processes, which can be achieved by studying a packed bed experimentally [69–71]. An adsorption column with a diameter of 0.7752 cm and a length of 4 cm was packed with 0.3 g of zeolites NaY synthesized from bagasse ash and rice husk ash, including modified zeolite NaY samples, before being placed in the tube furnace. The adsorption column was heated in a furnace connected to a CO₂ analyzer (Handheld CO₂ m GM 70, Helsinki, Finland).

In addition, Hedin and his colleagues [72] collected the CO₂ adsorption on various zeolite types; most of the results reported in the literature were obtained at temperatures between 273 and 298 K, whereas the flue gases are mainly emitted at a temperature above 573.15 K from the power plant. Therefore, adsorption experiments with pure CO₂ were performed at various temperatures (373.15, 573.15 and 873.15 K) and flow rates (1, 3 and 5 L/h). All samples were carried out at 1 atm with an adsorption time of 30 min.

The adsorbent samples were denoted as zeolite XSC-T-F. T represents the adsorption temperature, while F is the CO₂ flow rate of CO₂ adsorption in the pack bed reactor. Figure 1 shows the schematic diagram of the CO₂ adsorption test. The CO₂ adsorption capacity and breakthrough curve were defined in Equations (1) and (2).

$$q_e = \left(\frac{C_0 - C}{W} \right) \times V \times \frac{1}{M_W} \times t \quad (1)$$

$$\text{Breakthrough curve} = \frac{C}{C_0} \quad (2)$$

where q_e is the equilibrium adsorption capacity. C_0 and C are the concentrations of CO₂ at initial and after adsorption, respectively. The total flow rate is denoted by the abbreviation V . The molecular weight of the adsorbate is M_W . The weight of the adsorbent and the time are represented by W and t , respectively.

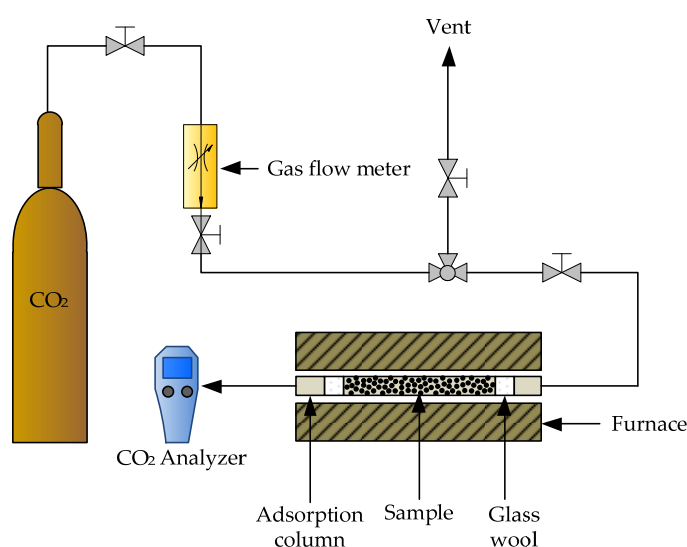


Figure 1. Schematic of CO₂ adsorption test in a packed bed reactor.

2.6. Characterization of Zeolite NaY

The chemical composition of bagasse ash and rice husk ash was evaluated by X-ray fluorescence spectroscopy (XRF; Bruker AXS, Karlsruhe, Germany). The result of this analysis was expressed as a percentage by the weight of oxides. The morphology and size of the obtained zeolites NaY, including modified zeolite, were determined via field emission scanning electron microscopy (FESEM; JSM-7001F, JEOL, Tokyo, Japan). The samples were coated with a thin layer of gold using a sputter coater (Edwards La-boratories, Milpitas, CA, USA) to improve their conductivity before the measurement. The elemental analysis of zeolite was carried out using energy dispersive X-ray spectroscopy (EDS; INCA PentaFETx3, Oxford Instruments Plc; Abington, UK). The crystallinity of zeolites NaY synthesized from bagasse ash and rice husk ash, including modified zeolite NaY was analyzed by XRD patterns using X-ray diffraction (XRD; Bruker AXS, Karlsruhe, Germany). The surface areas and porosity of the samples were examined by Brunauer–Emmett–Teller (BET) analysis (Autosorb 1C, Quantachrome, FL, USA) by nitrogen adsorption–desorption within the pores of the sample.

2.7. Statistical Analysis of the CO₂ Adsorption

The variation of variables under different conditions and their effects on the response variable have been considered according to available statistical tests in variance analysis. In this work, there are five variables, including the adsorbent, crystallization temperature of zeolite synthesis, wt.% of Zn loaded onto zeolite NaY, adsorption temperature and CO₂

flow rate. The considered factor of the adsorbent is the synthesis of zeolite NaY from different raw materials (bagasse ash and rice husk ash). The test ranges were varied as follows: 3 levels of crystallization temperatures at 298.15, 323.15 and 343.15 K, 3 levels of Zn loadings at 1, 3 and 5 wt.%, 3 levels of adsorption temperatures at 373.15, 573.15 and 873.15 K, and 3 levels of CO₂ flow rates of 1, 3 and 5 L/h. In this step, the data is entered into the Minitab software version 17 to conduct the variance analysis. The effect of all 5 variables on the CO₂ adsorption was investigated following the ANOVA and factorial design of experiments. Analysis of variance was employed to find out the significance of the main effect and interaction of factors involved, while the significance of the factors was determined by the probability values (*p*-values) of the models.

3. Results

3.1. Extracted Silica from Bagasse Ash and Rice Husk Ash

The chemical composition before silica extraction from bagasse ash showed that it contained 70.81, 17.40, 4.64, 4.34, and 2.81 wt.% of silicon dioxide (SiO₂), aluminum oxide (Al₂O₃), phosphorus pentoxide (P₂O₅), iron oxide (Fe₂O₃) and others, respectively. After silica extraction from bagasse ash was composed of 94.91, 2.81, 1.26 and 1.02 wt.% of SiO₂, Al₂O₃, P₂O₅ and Fe₂O₃, respectively. Moreover, XRF results showed that the rice husk ash was composed of 70.19, 23.40, 1.81, 1.67 and 2.93 wt.% of SiO₂, Al₂O₃, potassium oxide (K₂O), sodium oxide (Na₂O) and others, respectively. The extracted sample from rice husk ash consisted of 97.73, 2.24 and 0.03 wt.% of SiO₂, Al₂O₃ and Fe₂O₃, respectively. The amount of extracted silica from bagasse ash and rice husk ash was increased and it could be utilized to synthesize zeolite.

3.2. Synthesis of Zeolite NaY from Bagasse Ash and Rice Husk Ash

The crystallinity of pure zeolite NaY was confirmed using XRD patterns. Figure 2a shows the effect of crystallization temperatures on zeolite NaY derived from bagasse ash (B298, B323 and B343) and rice husk ash (R298, R323 and R343). The main peaks of all samples could be observed according to the standard peak of zeolite NaY (JCPDS 01-081-2466). The completion of the formation of the pure zeolite NaY phase was clearly demonstrated. The particles in all samples appeared to have spherical shapes and uniform distribution, as shown in SEM images from Figure 2b–g. The particle size distribution of zeolites B298, B323, B343, R298, R323 and R343 was approximately 0.28 ± 0.06 , 0.33 ± 0.02 , 0.37 ± 0.01 , 0.30 ± 0.04 , 0.35 ± 0.02 and 0.40 ± 0.05 μm in diameter, respectively. It was concluded that zeolite NaY was synthesized at a temperature of 298.15 K from bagasse ash and rice husk ash and crystallized to obtain a small crystal size. Consequently, the optimal crystallization temperature was 298.15 K with the highest BET surface area, micropore volume and total pore volume of both B298 and R298 zeolites.

3.3. Zeolite NaY Improvements

Figure 3a shows the XRD patterns of zeolites B298 and R298 that have improved properties with Zn loadings of 1 wt.% (1B298 and 1R298), 3 wt.% (3B298 and 3R298) and 5 wt.% (5B298 and 5R298). The XRD patterns for all modified zeolite NaY were similar to the standard peak of pure zeolite NaY; some diffraction peaks also matched the standard peak of ZnO (JCPDS 00-001-1136). SEM images of zeolites are shown in Figure 3b–g. The morphology of all samples was also characterized by spherical shaped crystals and uniform distribution. The crystal sizes of all the zeolites synthesized from bagasse ash and rice husk ash after being modified with Zn were approximately 0.25 ± 0.05 and 0.28 ± 0.07 μm in diameter, respectively.

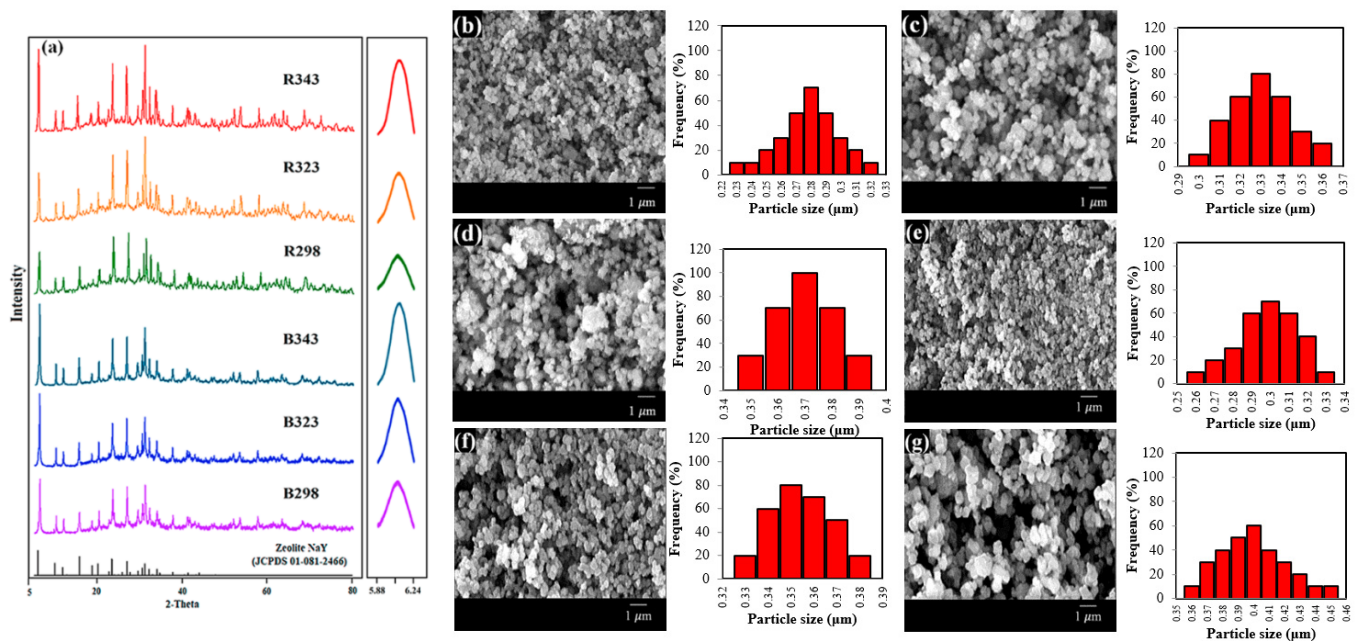


Figure 2. Zeolite NaY synthesized from bagasse ash and rice husk ash with different crystallization temperatures on XRD patterns, SEM images and particle size distribution: (a) XRD patterns, (b) B298, (c) B323, (d) B343, (e) R298, (f) R323 and (g) R343.

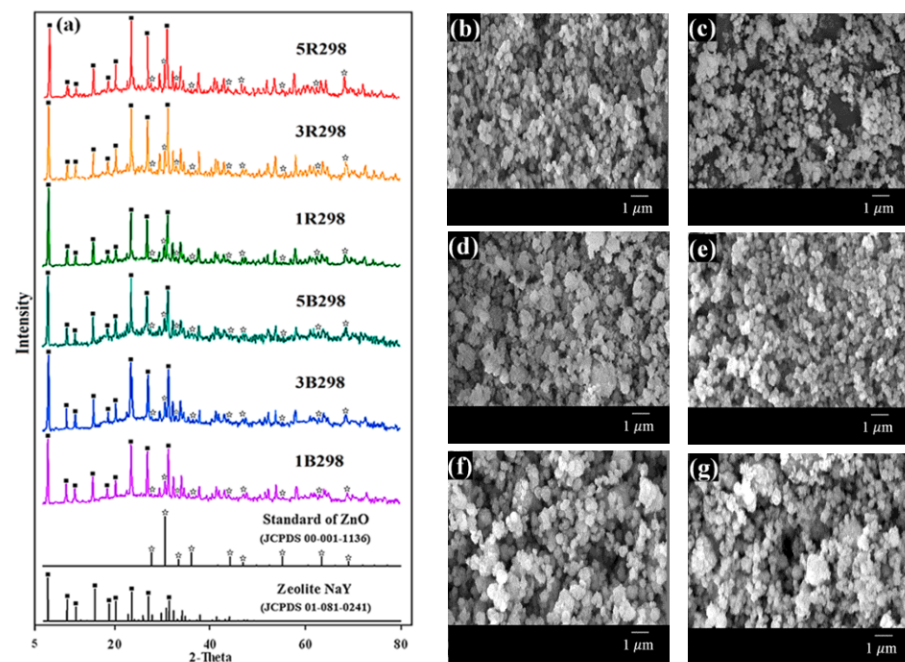


Figure 3. Zeolite NaY synthesized from bagasse ash and rice husk ash with different wt.% of Zn loadings on XRD patterns and SEM images: (a) XRD patterns, (b) 1B298, (c) 3B298, (d) 5B298, (e) 1R298, (f) 3R298 and (g) 5R298.

The elemental composition of the zeolites B298 and R298 after Zn loading was presented in Table 1 by EDS analysis. The elements O, Na, Al, Si and Zn were found in the zeolites B298 and R298 after Zn loading. The presence of Zn was confirmed by the fact that Zn^{2+} is ion-exchanged with Na^+ of the zeolites B298 and R298. It was clear that with an increase in the wt.% of Zn loading, the results of EDS showed the Zn at a high wt.%. It was

observed that approximately 0.99–5.15 wt.% Zn was successfully ion-exchanged in zeolites B298 and R298.

Table 1. EDS analysis of zeolite NaY synthesized from bagasse ash and rice husk ash with different wt.% of Zn loadings. The values are expressed in wt.%.

Sample	Si	Al	O	Na	Zn
1B298	12.16	16.11	56.14	14.46	1.13
3B298	12.23	16.13	57.85	10.69	3.10
5B298	12.08	16.21	58.33	8.23	5.15
1R298	12.36	16.48	56.13	14.04	0.99
3R298	12.18	16.20	57.14	11.59	2.89
5R298	12.28	16.44	57.52	8.56	5.20

The N₂ adsorption-desorption isotherms at 77 K for zeolite NaY synthesized from bagasse ash and rice husk ash with different wt.% of Zn loadings were shown in Figure 4. All the isotherms of the synthesized materials exhibited a Type I isotherm according to the IUPAC classification, which is characteristic of a microporous material and monolayer adsorption. The hysteresis loop was not found for these materials. Microporous material was adsorbed by the high volume of nitrogen at a low relative pressure around 0.02, followed by a moderate gradient in uptake until saturation pressure. This value agreed with a recent report by Salehi and Anbia [73].

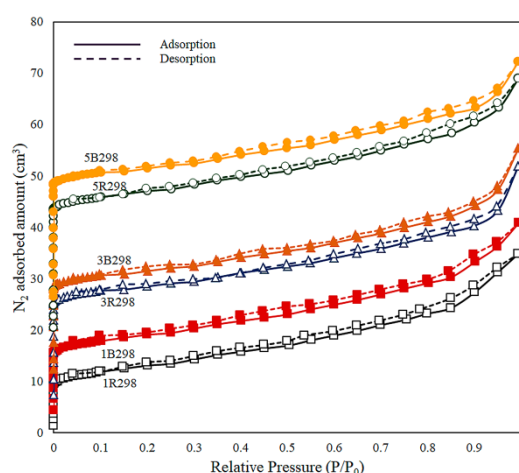


Figure 4. N₂ adsorption-desorption isotherms at 77 K for zeolite NaY synthesized from bagasse ash and rice husk ash with different wt.% of Zn loadings.

Moreover, the crystals corresponded to the results of the BET analysis, as shown in Table 2. It could be seen that the BET surface area, micropore volume and total pore volume of zeolites 1B298 and 1R298 were smaller than the zeolites 3B298, 3R298, 5B298 and 5R298. The result also showed that zeolites 5R298 and 5B298 had the highest BET surface area, micropore volume and total pore volume.

Table 2. BET analysis of zeolite NaY synthesized from bagasse ash and rice husk ash with different wt.% of Zn loadings.

Sample	Surface Area (m ² /g)	Micropore Volume (cm ³ /g)	Total Pore Volume (cm ³ /g)
1B298	39.86	0.020	0.163
3B298	54.39	0.025	0.229
5B298	71.14	0.030	0.291
1R298	34.57	0.018	0.137
3R298	50.71	0.023	0.205
5R298	68.75	0.028	0.264

3.4. CO₂ Adsorption Test

3.4.1. Effect of Crystallization Temperatures on the CO₂ Adsorption

The effects of raw materials and crystallization temperature in zeolite NaY synthesis on CO₂ adsorption were studied at a constant adsorption temperature of 573.15 K with a CO₂ flow rate of 5 L/h, as shown in Figure 5a. The zeolites B298-573-5 and R298-573-5 had the highest CO₂ adsorption capacities of 6.71 and 6.51 mmol/g, respectively. In addition, the breakthrough curves of CO₂ adsorption were presented in Figure 6a. It can be seen that the shape of the breakthrough curves of all samples initially increased rapidly, while the breakthrough curves of zeolites B298-573-5 and R298-573-5 showed a slower breakthrough speed than the other samples before becoming steady. This meant that zeolites B298-573-5 and R298-573-5 exhibited higher CO₂ adsorption capacities and a longer breakthrough time than the others. Therefore, the zeolites B298 and R298 were interested in testing the effect of Zn loading on CO₂ adsorption.



Figure 5. CO₂ adsorption capacity of zeolite NaY synthesized from bagasse ash and rice husk ash with different (a) crystallization temperatures, (b) wt.% of Zn loadings, (c) adsorption temperatures and (d) CO₂ flow rates.

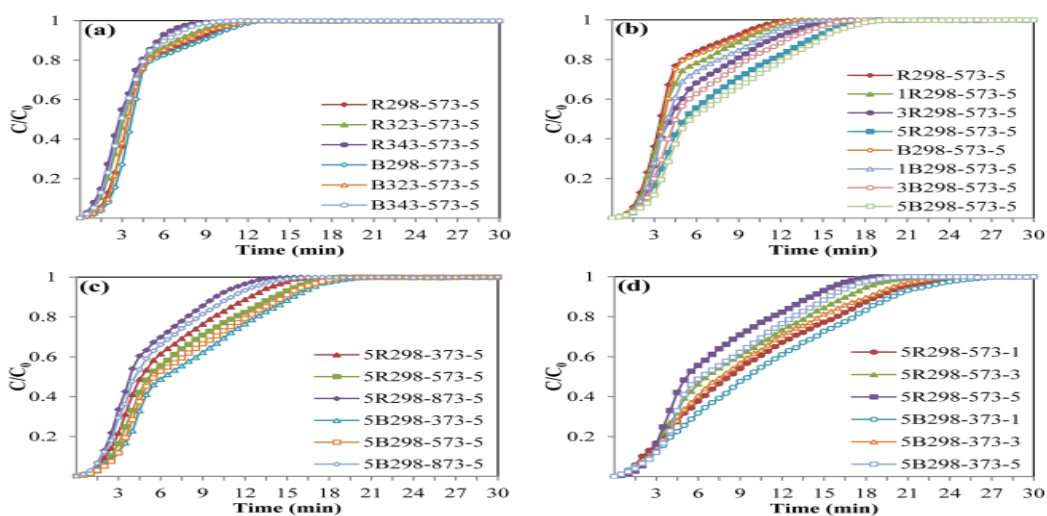


Figure 6. Breakthrough curves of zeolite NaY synthesized from bagasse ash and rice husk ash with different (a) crystallization temperatures, (b) wt.% of Zn loadings, (c) adsorption temperatures and (d) CO₂ flow rates.

3.4.2. Effect of Zn Loading on the CO₂ Adsorption

The effect of Zn loading on the CO₂ adsorption test was performed with different wt.% of Zn loadings (1, 3 and 5 wt.%) on zeolites B298 and R298 by fixing the adsorption temperature at 573.15 K and a CO₂ flow rate of 5 L/h, as shown in Figure 5b. At high wt.% Zn loading, the highest CO₂ adsorption capacity of 9.37 and 8.99 mmol/g was found on zeolites 5B298-573-5 and 5R298-573-5, respectively. Furthermore, the breakthrough curves of CO₂ adsorption are displayed in Figure 6b. It was found that the shape of the breakthrough curves of the zeolites 5B298-573-5 and 5R298-573-5 were not considerably altered at first. After the initial breakthrough, the breakthrough curves of zeolites 5B298-573-5 and 5R298-573-5 exhibited a slow breakthrough speed and then gradually became constant. For other samples, the breakthrough curve rapidly ascended and presented saturation trends. It showed a quick breakthrough speed, which could be due to the fastest diffusivity and the minimum equilibrium adsorption. It was found that the adsorption of zeolite NaY modified with Zn was higher than pure zeolite NaY. Therefore, the zeolites 5B298 and 5R298 were potential candidates to be studied under different operating conditions, including adsorption temperature and CO₂ flow rate.

3.4.3. Effect of Adsorption Temperature on the CO₂ Adsorption

Figure 5c shows the effect of adsorption temperature on the CO₂ adsorption test, including 373.15, 573.15 and 873.15 K on zeolites 5B298 and 5R298 by fixing the CO₂ flow rate of 5 L/h. The CO₂ adsorption capacity of zeolite 5B298-373-5 was found to be the highest at 9.45 mmol/g, shown in Figure 6c. The breakthrough curve of zeolite 5B298-373-5 and 5R298-373-5 at low temperatures exhibited a higher CO₂ adsorption capacity and a longer breakthrough time than the others. Therefore, the adsorption temperatures of 373.15 and 573.15 K were chosen to test the effect of CO₂ flow rate on the CO₂ adsorption of zeolites 5B298 and 5R298, respectively.

3.4.4. Effect of CO₂ Flow Rate on the CO₂ Adsorption

Figure 5d shows the effect of CO₂ flow rate on the CO₂ adsorption test with different CO₂ flow rates (1, 3 and 5 L/h) on zeolites 5B298 and 5R298 by fixing the adsorption temperatures at 373.15 and 573.15 K, respectively. At CO₂ flow rates of 1 L/h, the zeolites 5B298-373-1 and 5R298-573-1 exhibited the highest CO₂ adsorption capacities of 10.33 mmol/g and 9.91 mmol/g, respectively. Additionally, the breakthrough curves of CO₂ adsorption were presented and showed that the shape of the breakthrough curves of the zeolites 5B298-373-5 and 5R298-573-5 increased rapidly before becoming stable, as shown in Figure 6d. At a low flow rate, zeolites 5B298-373-1 and 5R298-573-1 exhibited the slowest breakthrough speed and then gradually stabilized, with the best CO₂ adsorbent among all tested materials of bagasse ash and rice husk ash, respectively.

3.5. Statistical Analysis of the CO₂ Adsorption

Minitab software version 17 was applied with ANOVA and factorial design of the experiment to determine model fitting, main effects and interactions between the dependent variables (responses) and independent variables (factors). The response variable was CO₂ adsorption, while the factors were the raw material, the crystallization temperature, wt.% of Zn loading, adsorption temperature and CO₂ flow rate.

3.5.1. Effects of Raw Material and Crystallization Temperature on the CO₂ Adsorption

The statistical significance was evaluated using a factorial design with different raw materials (bagasse ash and rice husk ash) and crystallization temperatures of zeolite synthesis (298.15, 323.15 and 343.15 K) on CO₂ adsorption occurring with a constant adsorption temperature at 573.15 K with a CO₂ flow rate of 5 L/h. As observed from Figure 7a, the variance analysis of data from experiments was normally distributed and independent, as evidenced by the fact that the points were close to a straight line. Figure 7b shows the main effects plot for each of the factors studied against the response variables. At the high

crystallization temperature of zeolite synthesis, the CO₂ adsorption decreased. On the other hand, at low crystallization temperatures, CO₂ adsorption increased. The interaction plots are presented in Figure 7c. There was no interaction between the factors of raw material and crystallization temperature of zeolite synthesis on CO₂ adsorption because of the perfect parallel lines in these plots.

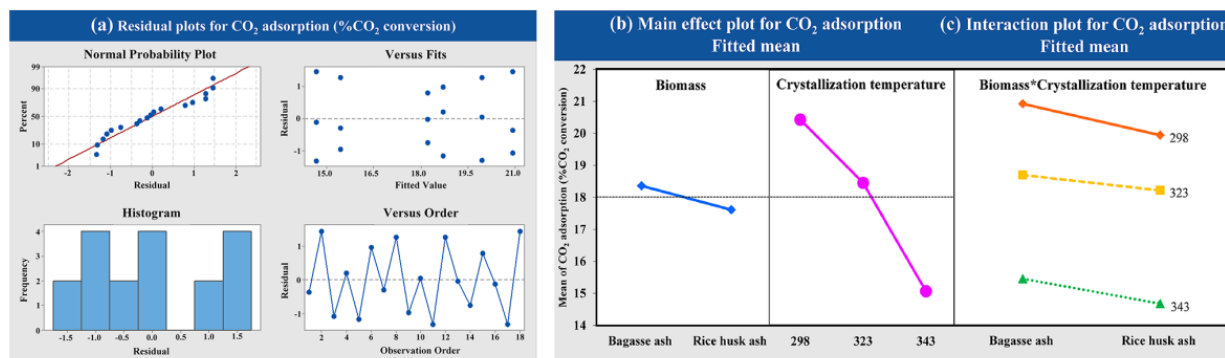


Figure 7. Results of (a) the variance analysis, (b) the main effects and (c) the interaction plot of the variable’s impact at different crystallization temperatures and raw materials for CO₂ adsorption.

3.5.2. Effects of Raw Material and Zn Loading on the CO₂ Adsorption

The effects of Zn loading on zeolite NaY (1, 3 and 5 wt.%) and raw material of zeolite synthesis (bagasse ash and rice husk ash) on CO₂ adsorption were studied using a factorial design of experiments. In order to examine the statistical significance of factor effects on the response variable, the adsorption temperature of 573.15 K with a CO₂ flow rate of 5 L/h was employed. The data analysis obtained from the experiment was normally distributed and independent, as shown in Figure 8a. At high wt.% of Zn loading on zeolite NaY, the CO₂ adsorption increased for both raw materials, as shown in Figure 8b. Figure 8c exhibited that there was no interaction between the factors of Zn loading on zeolite NaY and raw material for zeolite synthesis on CO₂ adsorption.

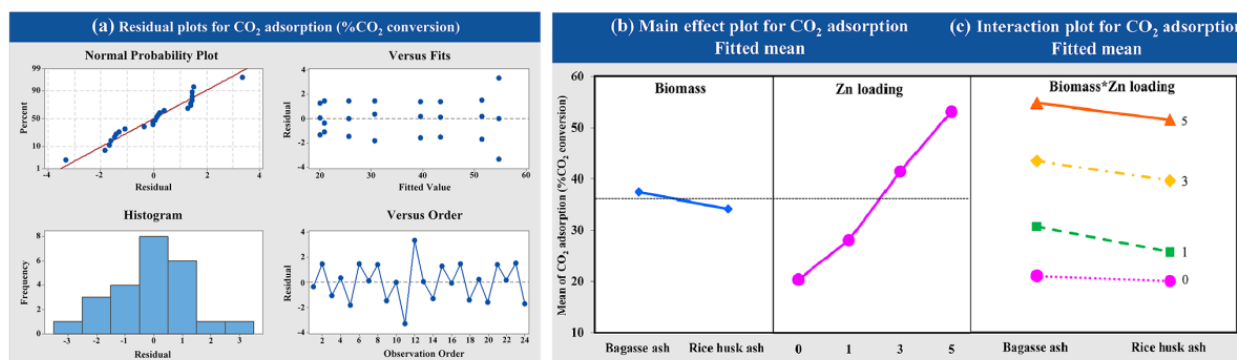


Figure 8. Results of (a) the variance analysis, (b) the main effects and (c) the interaction plot of the variable’s impact at different wt.% of Zn loadings and raw materials for CO₂.

3.5.3. Effects of Raw Material and of Adsorption Temperature on the CO₂ Adsorption

The factorial design was used to determine the statistical significance of CO₂ adsorption with different raw materials (bagasse ash and rice husk ash) and adsorption temperatures (373.15, 573.15 and 873.15 K) on CO₂ adsorption at a constant CO₂ flow rate of 5 L/h. Figure 9a exhibited that the data obtained were normally distributed and independent from variance analysis. CO₂ adsorption decreased at high adsorption temperatures, as illustrated in Figure 9b. Two factors of raw material and adsorption temperature interacted with each other as shown in Figure 9c. Analysis of interactions between the factors showed

that the response was dependent on the level of the factor. The highest CO₂ adsorption was found at 373.15 K and 573.15 K of adsorption temperature using adsorbents synthesized from bagasse ash and rice husk ash, respectively. The statistical results were according to the laboratory.

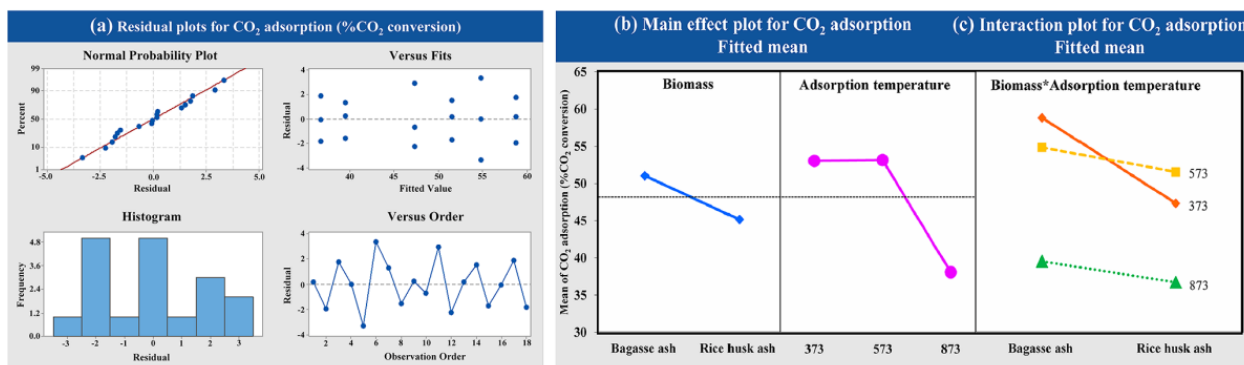


Figure 9. Results of (a) the variance analysis, (b) the main effects and (c) the interaction plot of the variable’s impact at different adsorption temperatures and raw materials for CO₂ adsorption.

3.5.4. Effects of Raw Material and CO₂ Flow Rate on the CO₂ Adsorption

The effects of CO₂ flow rate (1, 3 and 5 L/h) of 5 wt.% Zn/Y zeolites synthesized from bagasse ash and rice husk ash on the CO₂ adsorption were used for variance analysis following a single factor (one-way ANOVA). Figure 10a shows that the variance analysis of data obtained from experiments was normally distributed and independent. The interval plot for each level of the CO₂ flow rate on the CO₂ adsorption of 5 wt.% Zn/Y zeolite synthesized from bagasse ash and rice husk ash, as shown in Figure 10b,c. At a low CO₂ flow rate, the CO₂ adsorption increased. Lower CO₂ flow rate resulted in better CO₂ adsorption performances of 5 wt.% Zn/Y zeolite synthesized from both raw materials.

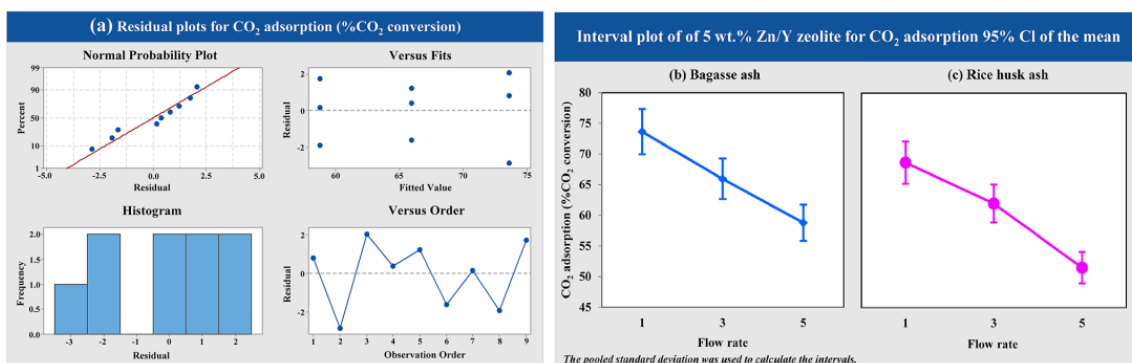


Figure 10. Results of (a) the variance analysis and the interval plot of 5 wt.% Zn/Y zeolite synthesized from (b) bagasse ash and (c) rice husk ash at different CO₂ flow rates for CO₂ adsorption.

4. Discussion

4.1. Silica Extraction from Bagasse Ash and Rice Husk Ash

XRF data revealed that the silica after extraction from bagasse ash and rice husk ash contained high silica content with a small amount of impurity. Bagasse ash and rice husk ash could be employed as an alternate silica source for zeolite NaY synthesis.

4.2. Synthesis of NaY Zeolite from Bagasse Ash and Rice Husk Ash

XRD patterns indicated that the crystallization rate was increased with increasing crystallization temperature, as evidenced by an increased degree of zeolite crystallinity with high peaks. Besides, it was indicated that as the crystallization temperature increased, the width of the peaks reduced, leading to enhanced crystal size. The SEM images of the

synthesized zeolites NaY showed crystal sizes corresponding to the research of Rakpasert (2012) [67]. The temperature of zeolite synthesis is an important factor in the crystallization rate and the resulting zeolite structure. At high crystallization temperatures of zeolite synthesis, it results in a high degree of zeolite crystallinity, which leads to large crystals being obtained. On the other hand, higher crystallization temperatures cause the aluminosilicate species to form dense arrangements, which preclude the creation of a porous structure [74]. The crystal sizes in this study correspond to the research of Koroglu and his colleagues [74]. They discovered that zeolite Y formed small crystals under a crystallization temperature of 4 and 25 °C. Consequently, the optimal crystallization temperature was 298.15 K because synthesis at 4 °C requires energy for temperature control. In addition, the crystal size of zeolite NaY synthesized from bagasse ash was higher than that of rice husk ash, which corresponds to increased BET surface area, micropore volume and total pore volume in BET analysis.

4.3. Zn Loading to Zeolite NaY

The crystalline structure of zeolite NaY synthesized from bagasse ash and rice husk ash was well-preserved after the incorporation of Zn into the zeolite NaY, according to XRD patterns for all samples. The decreased crystallinity depends on the increase of the percentage of Zn loading to zeolite NaY. The SEM images of modified zeolite NaY from bagasse ash and rice husk ash from this research were consistent with Ca-exchanged FAU and LTA-type zeolite from bagasse ash. They have reported that the particle size and shape were found to be unchanged after ion exchange [73]. Moreover, the crystals corresponded to the results of the BET analysis. The BET surface area, micropore volume and total pore volume were increased with an increase in Zn loading. Due to surface modification of the zeolite could enhance the alkalinity and cations incorporated into the zeolite structure [75,76]. The degree of ion exchange is determined by the metal ion size and charge [77]. The results of BET surface area, micropore volume and total pore volume of Zn loading on zeolites also showed higher than pure zeolites. This is because Zn modifies the surface charge properties of zeolites by producing Lewis acidic sites and redox features, according to Esquivel and his colleagues [56].

4.4. CO₂ Adsorption Test

4.4.1. Effect of Crystallization Temperature

The CO₂ adsorption capacity of zeolites NaY from bagasse ash and rice husk ash was increased with a decrease in the temperature of crystallization. The CO₂ adsorption capacity was increased when using bagasse ash for zeolite NaY synthesis because of its great physical properties. Furthermore, the variance analysis showed that factors of crystallization temperature significantly affected CO₂ adsorption, because the *p*-value was less than 0.05. This indicated that the increased crystallization temperature negatively affected the CO₂ adsorption. The interaction plots also indicated no interaction between factors of raw material and crystallization temperature of zeolite synthesis, the *p*-value of which was more than 0.05 (*p* = 0.937).

4.4.2. Effect of Zn Loading

The zeolite NaY modified with Zn exhibited a beneficial higher CO₂ adsorption capacity than pure zeolite, which corresponded to the BET analysis. The result also showed that the CO₂ adsorption capacity was increased with increasing the amount of Zn loading from 1 to 5 wt.% according to their physical properties. The increased surface area and total pore volume of zeolite NaY resulted in an increase in the number of adsorption sites for CO₂ adsorption, which corresponded to the research of Zhang et al. (2018) [78]. Figure 11 showed a possible mechanism for CO₂ adsorption on Zn/Y zeolite. The zeolite structure was composed of Na⁺ cations that are easily interchangeable with others to compensate for negative charge excess [54]. Two monovalent cations of Na⁺ must be replaced by a single divalent cation of Zn²⁺ to modify the surface charge characteristics of zeolite, resulting in a

high surface area and an electric field gradient within the pores and frameworks. When Zn/Y zeolite is used to adsorb CO₂, the Zn cation exhibits a stronger interaction with the CO₂ molecule, which leads to stronger CO₂ adsorption [57]. Due to the high surface area of the Zn/Y zeolite, there were more active sites on the zeolite [70]. The results agreed with the previous statistical analysis section. Based on the obtained results of the variance analysis, it was observed that the *p*-value was less than 0.05. The results of this analysis confirmed that Zn loading was statistically significant. The interaction plots showed that there was no interaction between the factors of Zn loading on zeolite NaY and raw material for zeolite synthesis on CO₂ adsorption (*p* = 0.311, which was more than 0.05).

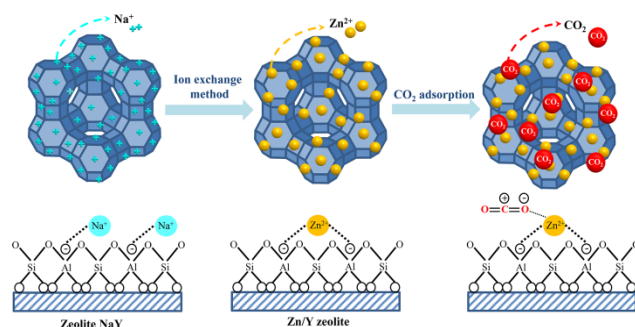


Figure 11. The possible mechanism for the CO₂ adsorption on Zn/Y zeolite.

4.4.3. Effect of Adsorption Temperature

The results indicated that at high adsorption temperatures, the CO₂ adsorption capacity decreased. Low adsorption temperatures resulted in physical adsorption rather than chemical adsorption. The surface area of the adsorbent, thus, holds an important role in the adsorption process at low temperatures when the adsorption temperature is increased [23,52,79]. The amount of CO₂ molecules adsorbed decreased at temperatures higher than 873.15 K, which corresponds to the research of Hedin and his colleagues [72]; its high number of adsorption sites and thermal conductivities corresponded to the research of Nyankson and his colleagues [23,52,77,79]. Moreover, the variance analysis revealed that the adsorption temperature was significant on CO₂ adsorption because the *p*-value was less than 0.05 (*p*-value = 0.000, which $\alpha = 0.05$). It was demonstrated that 873.15 K negatively affected the CO₂ adsorption. The interaction plots of two factors (raw material and adsorption temperature) showed interaction with each other because the *p*-value was less than 0.05 (*p* = 0.009, which $\alpha = 0.05$). This analysis confirmed that the raw material and the adsorption temperature had interacted with each other, and they affected the CO₂ adsorption of zeolite NaY.

4.4.4. Effect of CO₂ Flow Rate

The CO₂ adsorption with a CO₂ flow rate of 1 L/h was more than 0.25 times of 5 L/h. At a low CO₂ flow rate, the CO₂ adsorption was maintained over operating time. While the CO₂ flow rate was increased, the outflow CO₂ concentration increased, and total adsorption operating time was greatly reduced, according to the research from Cho et al. (2015) [80]. The residence time of the CO₂ flow rate at 1 L/h was longer than at 5 L/h. According to the research of Worathanakul and her colleagues [81], it could take more time to bind to CO₂ molecules, leading to enhanced CO₂ uptake. Analysis of variance results confirmed that the factors of CO₂ flow rate were statistically significant, with a *p*-value of the CO₂ flow rate factor less than 0.05. It was indicated that the increased CO₂ flow rate negatively affected CO₂ adsorption.

5. Conclusions

The zeolite NaY was successfully developed from bagasse ash and rice husk ash under the optimal crystallization temperature of 298.15 K. The formation of spherical-like crystals of zeolite NaY was confirmed by SEM images. The crystal size of the zeolite

NaY decreased with the decrease in crystallization temperature, which would result in better CO₂ adsorption performance. The crystal size and shape of the zeolite NaY did not change after being modified with Zn loading. The amount of Zn loading from modified NaY zeolite was higher in the BET surface area, micropore volume and total pore volume than pure zeolites. While a high wt.% of Zn loading on zeolite NaY resulted in good performance of CO₂ adsorption. The CO₂ adsorption capacity was also increased with the decrease in CO₂ flow rate and adsorption temperature. The highest CO₂ adsorption capacity was obtained at an adsorption temperature of 373.15 K and a CO₂ flow rate of 1 L/h on zeolite 5B298-373-1. In addition, the data on CO₂ adsorption capacities were analyzed in Minitab using a one-way ANOVA and a factorial design. In the CO₂ adsorption test, the types of adsorbents and adsorption temperature interaction were affected in CO₂ adsorption. Furthermore, the capacity of our advanced functionally synthesized zeolite NaY was higher than others and took a short time to crystallize the zeolite NaY at a low temperature. These characteristics suggested that bagasse ash and rice husk ash are eco-friendly and could be employed to decrease industrial pollution. They are also low-cost precursors and value-added materials as sustainable CO₂ adsorbent materials.

Author Contributions: Writing—original draft preparation, P.T.; Minitab software analysis, S.S.; writing—review and editing, P.W. All authors have read and agreed to the published version of the manuscript.

Funding: This research was funded by Thailand Research Fund (TRF), grant number PHD59I0018 and U-Thong biomass Company Limited.

Institutional Review Board Statement: Not applicable.

Informed Consent Statement: Not applicable.

Data Availability Statement: This study did not report any data.

Acknowledgments: We would like to thank the Graduate College at King Mongkut's University of Technology North Bangkok for supporting this research. We also to thank Khonburi Sugar Public Co., Ltd., Thailand for supporting materials used for experiments.

Conflicts of Interest: The authors declare no conflict of interest.

References

1. Zhao, Z.; Ma, C.; Chen, F.; Xu, G.; Pang, R.; Qian, X.; Shao, J.; Hu, X. Water caltrop shell-derived nitrogen-doped porous carbons with high CO₂ adsorption capacity. *Biomass Bioenergy* **2021**, *145*, 105969. [[CrossRef](#)]
2. Yang, P.; Rao, L.; Zhu, W.; Wang, L.; Ma, R.; Chen, F.; Lin, G.; Hu, X. Porous carbons derived from sustainable biomass via a facile one step synthesis strategy as efficient CO₂ adsorbents. *Ind. Eng. Chem. Res.* **2020**, *59*, 6194–6201. [[CrossRef](#)]
3. Ma, C.; Lu, T.; Shao, J.; Huang, J.; Hu, X.; Wang, L. Biomass derived nitrogen and sulfur co-doped porous carbons for efficient CO₂ adsorption. *Sep. Purif. Technol.* **2022**, *281*, 119899. [[CrossRef](#)]
4. Gavrilescu, D. Energy from biomass in pulp and paper mills. *Environ. Eng. Manag. J.* **2008**, *7*, 537–546. [[CrossRef](#)]
5. Kumar, A.; Kumar, N.; Baredar, P.; Shukla, A. A review on biomass energy resources, potential, conversion and policy in India. *Renew. Sustain. Energy Rev.* **2015**, *45*, 530–539. [[CrossRef](#)]
6. Office of the cane and sugar board. *International Sugar Statistics*; Ministry of Industry: Bangkok, Thailand, 2018. Available online: <http://www.ocsb.go.th> (accessed on 12 December 2021).
7. Prasara-A, J.; Gheewala, S.H. Sustainable utilization of rice husk ash from power plants: A review. *J. Clean. Prod.* **2017**, *167*, 1020–1028. [[CrossRef](#)]
8. Office of Agricultural Economics. *Agricultural Production Statistics*; Ministry of Agriculture and Cooperatives: Bangkok, Thailand, 2018. Available online: <https://www.oae.go.th/> (accessed on 12 December 2021).
9. Chauhan, M.K.; Chaudhary, V.S.; Samar, S.K. Life cycle assessment of sugar industry: A review. *Renew. Sustain. Energy Rev.* **2011**, *15*, 3445–3453. [[CrossRef](#)]
10. Nachat, N.; Tobameekul, P.; Worathanakul, P. Activated carbon from bagasse for syrup decolorization as an alternative for waste management and the assessment of carbon footprint. *Environ. Nat. Resour. J.* **2014**, *12*, 66–73.
11. Tippayawong, N.; Nakpan, K. Extended bagasse utilization for surplus electricity generation in sugar mills. In Proceedings of the International Conference on Green and Sustainable Innovation, Chiang Mai, Thailand, 29 November–1 December 2006.
12. Dias, M.O.D.S.; Filho, R.M.F.; Mantelatto, P.E.; Cavalett, O.; Rossell, C.E.V.; Bonomi, A.; Leal, M.R.L.V. Sugarcane processing for ethanol and sugar in Brazil. *Environ. Dev.* **2015**, *15*, 35–51. [[CrossRef](#)]

13. Na chat, N.; Maksiri, R.; Vichaikham, P.; Worathanakul, P. Carbon footprint of zeolite A and zeolite Y derived from bagasse ash for CO₂ adsorption. In Proceedings of the 11th International Conference on Life Cycle Assessment of Food in conjunction with the 6th LCA AgriFood Asia and 7th International Conference on Green and Sustainable Innovation, Bangkok, Thailand, 17–19 October 2018.
14. Katsuki, H.; Komarneni, S. Synthesis of Na-A and/or Na-X zeolite/porous carbon composites from carbonized rice husk. *J. Solid State Chem.* **2009**, *182*, 1749–1753. [[CrossRef](#)]
15. Yoon, S.J.; Son, Y.I.; Kim, Y.K.; Lee, J.G. Gasification and power generation characteristics of rice husk and rice husk pellet using a downdraft fixed-bed gasifier. *Renew. Energy* **2012**, *42*, 163–167. [[CrossRef](#)]
16. Panpa, W.; Jinawath, S. Synthesis of ZSM-5 zeolite and silicalite from rice husk ash. *Appl. Catal. B-Environ.* **2009**, *90*, 389–394. [[CrossRef](#)]
17. An, D.; Guo, Y.; Zhu, Y.; Wang, Z. A green route to preparation of silica powders with rice husk ash and waste gas. *Chem. Eng. J.* **2010**, *162*, 509–514. [[CrossRef](#)]
18. Wiśniewski, P.; Kistowski, M. Greenhouse gas emissions from cultivation of plants used for biofuel production in Poland. *Atmosphere* **2020**, *11*, 394. [[CrossRef](#)]
19. Kaithwas, A.; Prasad, M.; Kulshreshtha, A.; Verma, S. Industrial wastes derived solid adsorbents for CO₂ capture: A mini review. *Chem. Eng. Res. Des.* **2012**, *90*, 1632–1641. [[CrossRef](#)]
20. Worathanakul, P.; Tobameekul, P. Development of NaY zeolite derived from biomass and environmental assessment of carbon dioxide reduction. *MATEC Web Conf.* **2016**, *62*, 1–5. [[CrossRef](#)]
21. Worathanakul, P.; Kittipalarak, S.; Anusarn, K. Utilization biomass from bagasse ash for phillipsite zeolite synthesis. *Adv. Mater. Res.* **2011**, 383–390, 4038–4042.
22. Tadjarodi, A.; Haghverdi, M.; Mohammadi, V. Preparation and characterization of nano-porous silica aerogel from rice husk ash by drying at atmospheric pressure. *Mater. Res. Bull.* **2012**, *47*, 2584–2589. [[CrossRef](#)]
23. Wang, Y.; Du, T.; Qiu, Z.; Song, Y.; Che, S.; Fang, X. CO₂ adsorption on polyethylenimine-modified ZSM-5 zeolite synthesized from rice husk ash. *Mater. Chem. Phys.* **2018**, *207*, 105–113. [[CrossRef](#)]
24. Liou, T.H. Preparation and characterization of nano-structured silica from rice husk. *Mater. Sci. Eng. A* **2004**, *364*, 313–323. [[CrossRef](#)]
25. Worathanakul, P.; Layakul, T.; Juengsura, P. Kinetic model of nitric oxide reduction on CuFe/SUZ-4 catalyst in packed bed column. *Int. J. Chem. Eng. Appl.* **2015**, *6*, 450–454. [[CrossRef](#)]
26. Papailias, G.; Mavroidis, I. Atmospheric emissions from oil and gas extraction and production in Greece. *Atmosphere* **2017**, *9*, 152. [[CrossRef](#)]
27. Hu, Y.; Shi, Y. Estimating CO₂ emissions from large scale coal-fired power plants using OCO-2 observations and emission inventories. *Atmosphere* **2021**, *12*, 811. [[CrossRef](#)]
28. Patiño, L.I.; Padilla, E.; Alcántara, V.; Raymond, J.L. The relationship of energy and CO₂ emissions with GDP per capita in Colombia. *Atmosphere* **2020**, *11*, 778. [[CrossRef](#)]
29. Zarifi, M.H.; Shariaty, P.; Hashisho, Z.; Daneshmand, M. A non-contact microwave sensor for monitoring the interaction of zeolite 13X with CO₂ and CH₄ in gaseous streams. *Sens. Actuators B Chem.* **2017**, *238*, 1240–1247. [[CrossRef](#)]
30. Abid, H.R.; Rada, Z.H.; Shang, J.; Wang, S. Synthesis, characterization, and CO₂ adsorption of three metal-organic frameworks (MOFs) MIL-53, MIL-96, and amino-MIL-53. *Polyhedron* **2016**, *120*, 103–111. [[CrossRef](#)]
31. Song, G.; Zhu, X.; Chen, R.; Liao, Q.; Ding, Y.-D.; Chen, L. An investigation of CO₂ adsorption kinetics on porous magnesium oxide. *Chem. Eng. J.* **2016**, *283*, 175–183. [[CrossRef](#)]
32. IPCC (Intergovernmental Panel on Climate Change). *Climate Change 2007: The Physical Science Basis. Contribution of Working Group I to the Fourth Assessment Report of the Intergovernmental Panel on Climate Change*; Cambridge University Press: Cambridge, UK, 2007.
33. Wang, M.; Lawal, A.; Stephenson, P.; Sidders, J.; Ramshaw, C.; Yeung, H. Post-combustion CO₂ capture with chemical absorption: A state-of-the-art review. *Chem. Eng. Res. Des.* **2011**, *89*, 1609–1624. [[CrossRef](#)]
34. Chen, H.; Wang, W.; Ding, J.; Wei, X.; Lu, J. CO₂ adsorption capacity of FAU zeolite in presence of H₂O a monte carlo simulation study. *Energy Procedia* **2017**, *105*, 4370–4376. [[CrossRef](#)]
35. Vinoba, M.; Bhagiyalakshmi, M.; Alqaheem, Y.; Alomair, A.A.; Pérez, A.; Rana, M.S. Recent progress of fillers in mixed matrix membranes for CO₂ separation: A review. *Sep. Purif. Technol.* **2017**, *188*, 431–450. [[CrossRef](#)]
36. Raganati, F.; Alfe, M.; Gargiulo, V.; Chirone, R.; Ammendola, P. Isotherms and thermodynamics of CO₂ adsorption on a novel carbon-magnetite composite sorbent. *Chem. Eng. Res. Des.* **2018**, *134*, 540–552. [[CrossRef](#)]
37. Liang, Z.; Marshall, M.; Chaffee, A.L. Comparison of Cu-BTC and zeolite 13X for adsorbent based CO₂ separation. *Energy Procedia* **2009**, *1*, 1265–1271. [[CrossRef](#)]
38. Banihashemi, F.; Pakizeh, M.; Ahmadpour, A. CO₂ separation using PDMS/ZSM-5 zeolite composite membrane. *Sep. Purif. Technol.* **2011**, *79*, 293–302. [[CrossRef](#)]
39. Moura, P.A.S.; Bezerra, D.P.; Villarrasa-Garcia, E.; Bastos-Neto, M.; Azevedo, D.C.S. Adsorption equilibria of CO₂ and CH₄ in cation-exchanged zeolites 13X. *Adsorption* **2016**, *22*, 71–80. [[CrossRef](#)]
40. Liu, X.; Zhou, L.; Fu, X.; Sun, Y.; Su, W.; Zhou, Y. Adsorption and regeneration study of the mesoporous adsorbent SBA-15 adapted to the capture/separation of CO₂ and CH₄. *Chem. Eng. Sci.* **2007**, *62*, 1101–1110. [[CrossRef](#)]

41. Zhao, Z.; Cui, X.; Ma, J.; Li, R. Adsorption of carbon dioxide on alkali-modified zeolite 13X adsorbents. *Int. J. Greenh. Gas Control* **2007**, *1*, 355–359. [[CrossRef](#)]
42. Grande, C.A.; Rodrigues, A.E. Electric swing adsorption for CO₂ removal from flue gases. *Int. J. Greenh. Gas Control* **2008**, *2*, 194–202. [[CrossRef](#)]
43. Grant, G.T.; Dunne, K.I.; Davis, R.J.; LeVan, M.D. Carbon-silica composite adsorbent: Characterization and adsorption of light gases. *Micropor. Mesopor. Mater.* **2008**, *111*, 1–11.
44. Gray, M.L.; Champagne, K.J.; Fauth, D.; Baltrus, J.P.; Pennline, H. Performance of immobilized tertiary amine solid sorbents for the capture of carbon dioxide. *Int. J. Greenh. Gas Control* **2008**, *2*, 3–8. [[CrossRef](#)]
45. Subagyono, D.J.N.; Liang, Z.; Knowles, G.P.; Chaffee, A.L. Amine modified mesocellular siliceous foam (MCF) as a sorbent for CO₂. *Chem. Eng. Res. Des.* **2011**, *89*, 1647–1657. [[CrossRef](#)]
46. Rajamani, K.; Jasper, M.V.B. A comparison of the CO₂ capture characteristics of zeolites and metal-organic frameworks. *Sep. Purif. Technol.* **2012**, *87*, 120–126.
47. Shafeeyan, M.S.; Daud, W.M.A.W.; Shamiri, A.; Aghamohammadi, N. Adsorption equilibrium of carbon dioxide on ammonia-modified activated carbon. *Chem. Eng. Res. Des.* **2015**, *104*, 42–52. [[CrossRef](#)]
48. Rad, M.D.; Fatemi, S.; Mirfendereski, S.M. Development of T type zeolite for separation of CO₂ from CH₄ in adsorption processes. *Chem. Eng. Res. Des.* **2012**, *90*, 1687–1695. [[CrossRef](#)]
49. Chang, H.L.; Dong, H.H.; Hyunchul, J.; Wonkeun, C.; Dong, H.J.; Dong, K.S.; Sung, H.K. Effects of pore structure and PEI impregnation on carbon dioxide adsorption by ZSM-5 zeolites. *J. Ind. Eng. Chem.* **2015**, *23*, 251–256.
50. Worathanakul, P.; Rakpasert, N. Different preparation methods of Ni-FAU(Y) zeolite for nitric oxide reduction. *Int. J. Chem. Eng. Appl.* **2019**, *10*, 106–109. [[CrossRef](#)]
51. Bezerra, D.P.; Oliveira, R.S.; Vieira, R.S.; Cavalcante, C.L., Jr.; Azevedo, D.C.S. Adsorption of CO₂ on nitrogen-enriched activated carbon and zeolite 13X. *Adsorption* **2011**, *17*, 235–246. [[CrossRef](#)]
52. Ammendola, P.; Raganati, F.; Chirone, R. CO₂ adsorption on a fine activated carbon in a sound assisted fluidized bed: Thermodynamics and kinetics. *Chem. Eng. J.* **2017**, *322*, 302–313. [[CrossRef](#)]
53. Grande, C.A.; Kvamsdal, H.; Mondino, G.; Blom, R. Development of moving bed temperature swing adsorption (MBTSA) process for postcombustion CO₂ capture: Initial benchmarking in a NGCC context. *Energy Procedia* **2017**, *114*, 2203–2210. [[CrossRef](#)]
54. Lee, S.Y.; Park, S.J. A review on solid adsorbents for carbon dioxide capture. *J. Ind. Eng. Chem.* **2015**, *23*, 1–11. [[CrossRef](#)]
55. Worathanakul, P.; Rakpasert, N. Influence of different preparation methods of copper loading on Na-Y zeolite for green gas emission. *Int. J. Environ. Sci. Dev.* **2016**, *7*, 885–888. [[CrossRef](#)]
56. Esquivel, D.; Cruz-Cabeza, A.J.; Jiménez-Sanchidrián, C.; Romero-Salguero, F.J. Transition metal exchanged β zeolites: Characterization of the metal state and catalytic application in the methanol conversion to hydrocarbons. *Micropor. Mesopor. Mater.* **2013**, *179*, 30–39. [[CrossRef](#)]
57. Smykowski, D.; Szyja, B.; Szczygieł, J. DFT modeling of CO₂ adsorption on Cu, Zn, Ni, Pd/DOH zeolite. *J. Mol. Graph. Model.* **2013**, *41*, 89–96. [[CrossRef](#)] [[PubMed](#)]
58. Wardono, A.; Agoestanto, A.; Rosidah, S. Arima method with the software minitab and eviews to forecast inflation in Semarang Indonesia. *J. Theor. Appl. Inf. Technol.* **2016**, *94*, 61–76.
59. Ziari, H.; Farahani, H.; Goli, A. Using the statistical analysis of carbon nano-tubes dispersion in bitumen employing software MINITAB. *Int. J. Transp. Eng.* **2013**, *1*, 125–136.
60. Baldovino, F.H.B.; Dugos, N.P.; Roces, S.A.; Quitain, A.T.; Kida, T. Process optimization of carbon dioxide adsorption using nitrogen-functionalized graphene oxide via response surface methodology approach. *Am. J. Chem. Eng.* **2017**, *17*, 106–113. [[CrossRef](#)]
61. Gunawan, T.J.; Ikhwan, Y.; Restuhadi, F.; Pato, U. Effect of light Intensity and photoperiod on growth of *Chlorella pyrenoidosa* and CO₂ Biofixation. *E3S Web Conf.* **2018**, *31*, 1–7.
62. Pedraza, J.I.; Suarez, L.A.; Martinez, L.A.; Rojas, N.Y.; Tobon, J.I.; Ramirez, J.H.; Zea, H.R.; Caceres, A.A. Carbon capture and utilization by mineral carbonation with CKD in aqueous phase: Experimental stage and characterization of carbonated products. In Proceedings of the 7th International Workshop, Advances in Cleaner Production, Academic Work, Barranquilla, Colombia, 21–22 June 2018.
63. Rodríguez-Mosqueda, R.; Bramer, E.A.; Brem, G. CO₂ capture from ambient air using hydrated Na₂CO₃ supported on activated carbon honeycombs with application to CO₂ enrichment in greenhouses. *Chem. Eng. Sci.* **2018**, *189*, 114–122. [[CrossRef](#)]
64. Thompson, W.A.; Perier, C.; Maroto-Valer, M.M. Systematic study of sol-gel parameters on TiO₂ coating for CO₂ photoreduction. *Appl. Catal. B-Environ.* **2018**, *238*, 136–146. [[CrossRef](#)]
65. Mohammad, A.F.; El-Naas, M.H.; Suleiman, M.I.; Musharfy, M.A. Optimization of a Solvay-Based Approach for CO₂ Capture. *Int. J. Chem. Eng. Appl.* **2016**, *7*, 230–234. [[CrossRef](#)]
66. El-Azazy, M.; El-Shafie, A.S.; Issa, A.A.; Al-Sulaiti, M.; Al-Yafie, J.; Shomar, B.; Al-Saad, K. Potato peels as an adsorbent for heavy metals from aqueous solutions: Eco-structuring of a green adsorbent operating Plackett-Burman Design. *J. Chem.* **2019**, *2019*, 1–14. [[CrossRef](#)]
67. Rakpasert, N. Preparation of Different Metals Loading on FAU Zeolite for NO Reduction. Master's Thesis, King Mongkut's University of Technology North Bangkok, Bangkok, Thailand, 2012.

68. Worathanakul, P.; Saisuwanisiri, P. Effect of copper and iron loading on zeolite Y for carbon dioxide adsorption. *J. King Mongkut's Univ. Technol. N. Bangk.* **2017**, *28*, 373–381. [[CrossRef](#)]
69. Nikolaidis, G.N.; Kikkinides, E.S.; Georgiadis, M.C. A model-based approach for the evaluation of new zeolite 13X-based adsorbents for the efficient post-combustion CO₂ capture using P/VSA processes. *Chem. Eng. Res. Des.* **2018**, *131*, 362–374. [[CrossRef](#)]
70. Park, Y.; Ju, Y.; Park, D.; Lee, C.-H. Adsorption equilibria and kinetics of six pure gases on pelletized zeolite 13X up to 1.0 MPa: CO₂, CO, N₂, CH₄, Ar and H₂. *Chem. Eng. J.* **2016**, *292*, 348–365. [[CrossRef](#)]
71. Liu, S.; Rao, L.; Yang, P.; Wang, X.; Wang, L.; Ma, R.; Yue, L.; Hu, X. Superior CO₂ uptake on nitrogen doped carbonaceous adsorbents from commercial phenolic resin. *J. Environ. Sci.* **2002**, *93*, 109–116. [[CrossRef](#)]
72. Hedin, N.; Andersson, L.; Bergström, L.; Yan, J. Adsorbents for the post-combustion capture of CO₂ using rapid temperature swing or vacuum swing adsorption. *Appl. Energy* **2013**, *104*, 418–433. [[CrossRef](#)]
73. Salehi, S.; Anbia, M. Characterization of CPs/Ca-exchanged FAU- and LTA-type zeolite nanocomposites and their selectivity for CO₂ and N₂ adsorption. *J. Phys. Chem. Solids* **2017**, *110*, 116–128. [[CrossRef](#)]
74. Koroğlu, H.J.; Sarioğlu, A.; Tatlier, M.; Erdem-Şenatalar, A.; Savaşçı, Ö.T. Effects of low-temperature gel aging on the synthesis of zeolite Y at different alkalinities. *J. Cryst. Growth* **2002**, *241*, 481–488. [[CrossRef](#)]
75. Younas, M.; Sohail, M.; Leong, L.K.; Bashir, M.J.K.; Sumathi, S. Feasibility of CO₂ adsorption by solid adsorbents: A review on low-temperature systems. *Int. J. Environ. Sci. Technol.* **2016**, *13*, 1839–1860. [[CrossRef](#)]
76. Diaz, E.; Munoz, E.; Vega, A.; Ordonez, S. Enhancement of the CO₂ retention capacity of X zeolites by Na- and Cs-treatments. *Chemosphere* **2008**, *70*, 1375–1382. [[CrossRef](#)]
77. Nyankson, E.; Efavi, J.K.; Yaya, A.; Manu, G.; Asare, K.; Daafuor, J.; Abrokwah, R.Y. Synthesis and characterisation of zeolite-A and Zn-exchanged zeolite-A based on natural aluminosilicates and their potential applications. *Cogent Eng.* **2018**, *5*, 1–23. [[CrossRef](#)]
78. Zhang, S.; Zhao, Y.; Yang, J.; Zhang, J.; Zheng, C. Fe-modified MnOx/TiO₂ as the SCR catalyst for simultaneous removal of NO and mercury from coal combustion flue gas. *Chem. Eng. J.* **2018**, *348*, 618–629. [[CrossRef](#)]
79. Ramasubramanian, K.; Severance, M.A.; Dutta, P.K.; Ho, W.S.W. Fabrication of zeolite/ polymer multilayer composite membranes for carbon dioxide capture: Deposition of zeolite particles on polymer supports. *J. Colloid Interface Sci.* **2015**, *452*, 203–214. [[CrossRef](#)] [[PubMed](#)]
80. Cho, Y.; Lee, J.Y.; Bokare, A.D.; Kwon, S.B.; Park, D.S.; Jung, W.S.; Choi, J.S.; Yang, Y.M.; Lee, J.Y.; Choi, W. LiOH-embedded zeolite for carbon dioxide capture under ambient conditions. *J. Ind. Eng. Chem.* **2015**, *22*, 350–356. [[CrossRef](#)]
81. Worathanakul, P.; Klinpol, N.; Sarai, T. Innovation of CO₂ adsorption with Li/zeolite A derived from bagasse ash. In Proceedings of the Universal Academic Cluster International Spring Conference in Osaka, Osaka, Japan, 12–14 April 2017.